DETERMINATION OF FRACTURE MECHANICS VALUES BY DIFFERENT SPECIMEN TYPES AND IT'S USE FOR SAFETY ANALYSES

A. Heuser*, W. Dahl*

Fracture mechanic tests using CT- and 3 SENB-specimens were performed to find out whether there exists an influence caused by the specimen type. Results are presented for steels with different strength levels tested in the elasto-plastic as well as in the linear elastic regime of material behaviour. The crack resistance behaviour was determined using different specimen types. The results are finally used to show how far a safety analyses is influenced by the different fracture mechanics values.

INTRODUCTION

Fracture mechanic values are often determined with different specimen geometries. These differ not only in dimensions but also in loading conditions. CT- and 3 SENB-specimens are most common to determine fracture mechanics values in the linear-elastic as well as in the elasto plastic regime of material behaviour. The specimen type is often selected by considerations like how to save material and money. This proceeding seems to be justified because the evaluated fracture mechanics data should not depend on specimen type within the validity range of fracture mechanics concepts like K_{Ic} and J-integral.

One result of J_R-curve evaluation on HY 130 steel by an ASTM round robin (1) was that 3 SENB-specimens resulted in J_R-curves with a steeper slope compared to CT-specimens of same thickness. Jones et al. (2) evaluated the same differences in stable crack growth resistance behaviour on a copper-nickel alloy. Garwood (3) determined for center-notched-tension and bend samples J_{Ic}-values which coincide but different slopes of J_R-curves were observed.

* Institute for Ferrous Metallurgy at Technical University, Aachen, FRG

The differences in the evaluated J_R-curves described in (1) and (2) are also present if the limitations of J-controlled crack growth are taken into account. The criteria describing the validity range of J-integral is formulated for bend specimens as:

$$Z > 25\ J\ (0{,}5\ (\sigma_{ys} + \sigma_{UTS}))^{-1} \quad (1)$$

$$\Delta a < 0{,}06\ Z \quad (2)$$

$$dJ/da > \omega J\ (W-a)^{-1} \quad (3)$$

with $\omega >> 1$ often $\omega = 10$

$Z = a, (W-a), B$

The purpose of the work reported here is to find out whether there exists an influence in the description of toughness behaviour caused by the specimen type. Therefore fracture mechanics tests using CT- and 3 SENB-specimens were performed on steels with different strength levels.

Materials and Specimen Dimensions

The tests were carried out using 40 mm thick plates of the steels Fe E 470, Fe E 460 and Fe E 690. While the plates of Fe E 470 and Fe E 690 were in quenched and tempered condition the plate of Fe E 460 steel was normalized. 3 SENB-samples with a thickness B = 35 mm and a width of W = 70 mm as well as CT-specimens of the same thickness and a width of W=80 mm were prepared. Additionally 1 CT- (B = 25 mm), 2 CT- (B = 28 mm), 4 SENB and 3 SENB-samples (B = 25 mm, W = 2B) were produced out of a 30 mm thick quenched and tempered plate of 20 MnMoNi 5 5 steel. The chemical compositions and mechanical properties for the three steels of investigation are listed in table 1. Specimens were tested with 20% side grooves and without. This procedure was chosen to avoid shear lip formation and to produce plane strain conditions, taking into account results of finite element computations done by de Lorenzi et al. (4). Side grooving was performed after prefatiguing plain sided specimens. To be sure that the fatigue crack was situated very well in the side grooved plane the specimens were fatigue loaded again to the last load. All specimens were prefatigued to an a/W-ratio of about 0.53.

Test and Evaluation

The fracture mechanics tests were carried out in displacement control using servo-hydraulic testing machines (100 kN and 1000 kN). J-integral values were estimated following the procedure given in ASTM E 813. In order to measure the load point deflection of the 3 SENB-specimens the reference bar method proposed by Dawes (5) was used.

The crack tip opening displacement (CTOD) was calculated by the formalism given by the British standard BS 5762. The extrapolation formula given in this standard is only valid for 3 SENB-specimens. But nevertheless it seems to be possible to use it also for CT-specimens. There are published results (6) which show a good agreement between CTOD values obtained by this formalism and those obtained from silicon replica technique testing CT-samples.

RESULTS

Behaviour in the Linear Elastic and in the Elastic-Plastic range

Figure 1 shows results of fracture mechanics tests done in a temperature range from 77 K to RT on 20 MnMoNi 5 5 steel. The plotted data were evaluated for the maximum load. Additionally J_i-values describing the beginning of stable crack growth were estimated using DC-potential technique. Within the scatter of such values no significant differences were observed for the J_i-data obtained by the different specimen types.

In the temperature range where the specimens failed by unstable cleavage fracture the J-integral values of plain sided CT- and 3 SENB-samples were very similar. Compared to this result there is to notice a tendency of a decrease in J-integral values using side grooved CT-specimens. CT-specimens notched by a saw cut (notch radius 0.05 mm) showed a tendency to higher J-integral data. The K_{Ic}-value estimated at 77K using such a sample is twice of the K_{Ic} of a fatigue cracked specimen (7).

The temperature T_j describing the beginning of stable crack growth is the same for plain sided CT- and 3 SENB samples. But T_i will be shifted to higher values using side grooved samples. Notched specimens show a contrary behaviour.

In the temperature region higher than T_j the specimens failed after some amount of stable crack growth. The J_{max}-values estimated for 3 and 4 SENB-specimens are clearly higher than for CT-specimens. All relevant dimensions of the specimens were similar. Therefore it seems to be allowed to compare the values quantitatively. Side grooved, plain sided and notched CT-specimens have the same level of J_{max}, J_u-data.

The notch radius of specimens prepared by a saw cut is smaller than the critical width of the stretched zone, CTOD at initiation. This gives an explanation that you will get the same specimen behaviour compared to prefatigue cracked bodies (7).

The differences in J_{max}-values using CT- or 3 SENB were also present if the test data were used to estimate CTOD values (8). Results of fracture mechanics tests on the steels Fe E 460 and

Fe E 470 performed at different temperatures are shown in figure 2 and 3 which show the CTOD values estimated at the failure of 3 SENB- and CT-specimens respectively. Great differences of CTOD data are obvious in the temperature range where failure occurs after some amount of stable crack growth. It is more dramatic for the results on Fe E 460 steel, figure 3. δ_i-values, CTOD at stable crack initiation, are very close together in the case of Fe E 460 steel. But FeE 470 steel showed some difference in δ_i-data using CT-or 3 SENB-specimens, figure 2. It is not quite clear whether it is due to some scatter caused by the potential method or to a real effect. The temperature T_i and the δ_c-values are not affected by specimen type.

Crack Resistance Behaviour

The differences in CTOD- and J-integral values described appear only in the temperature range where the specimens failure is caused by some amount of stable crack growth. Therefore J_R-curves were determined using SENB- and CT-samples. The results are presented for four different steels with different strength levels in figure 4 to 7. The J_R-curves were obtained using multiple-specimen technique according to ASTM standard. A power law fit was used to describe the crack growth resistance behaviour.

Compared to CT-specimens the SENB-specimens result in J_R-curves with higher J-integral values and a steeper slope. If side grooved SENB-specimens were used the slope of J_R-curves decreased. Then the test data correspond to those of plain sided CT-samples considering the scatter of results. Side grooving of CT-specimens resulted in a small decrease of J_R-curves. But the differences with plain sided CT-samples are small. Testing side grooved SENB-specimens resulted in J_R-curves which are very close to the CT-ones. Differences in J_R-curves using plain sided CT- or SENB-specimens did not occur in the same manner for all materials investigated. Figure 7 shows that for Fe E 690 steel only very small differences were observed in the description of stable crack growth. In figure 4 to 7 the conditions of J-controlled crack growth formulated in equation (1) to (3) are marked. Also if these limitations are taken into account, a specimen type dependence of results is to notice.

In an earlier work (7) it was shown that 3 SENB-specimens notched by a small saw cut resulted in the same J_R-curve than using prefatigue cracked sampels. As mentioned before this behaviour is due to the fact that the notch radius produced is smaller than the δ_i-values.

The estimation method for J_{IC}-values given in ASTM E 813 has been critized a lot (9) because it uses a linear fit of test data and a blunting line which considers the hardening behaviour of materials only by a mean value of σ_{ys} and σ_{UTS}. Therefore in figure

4 to 7 are drawn in blunting lines which can be derived using relationships given by Shih et al. (10) based on HRR-field equations. These blunting lines depend on the hardening behaviour of the material itself described by the parameters α and N of Ramberg-Osgood law, on the stress state and on the ratio σ_{ys}/E. These "HRR-field" blunting lines seem to describe the blunting phase within the J_R-curves better than the ASTM ones. No data point in figure 4 to 7 is on the left hand side of "HRR-field" blunting lines determined on specimens which showed some amount of stable crack growth. Whereas the blunting of the crack tip calculated by the ASTM E 813 overestimates the blunting behaviour of the materials.

Prediciton of Failure Behaviour Using Fracture Mechanics Test Results

It is necessary for a safety analyses to compare the loading situation of the construction with suitable material values. For that purpose elasto-plastic fracture mechanics material values are used like J-integral and CTOD. The construction behaviour is characterised by exact FE-calculations (11) or approaching procedures like "Two-Criteria-Approach" (12), "Engineering-Approach" (13) and "Burdekin-Dawes-Design-Concept" (14).

The CTOD test results were used to predict maximum allowable crack lengths a_{crit} using the CTOD-Design-Concept. The estimation procedure formulated in PD 6493 (14) was used. The calculations were done for a fictive part of a construction containing a crack which length is small compared to the width. That means an a/W-ratio of $a/W \leq 0.1$. It was assumed that the construction is loaded to 90% of the yield strength of the material. $CTOD_{max}$-values were used, determined on the steels Fe E 470, Fe E 460 and 20 MnMoNi 55 at RT. Figure 8 shows a comparison of calculated allowable crack lengths a_{crit} using $CTOD_{max}$-data obtained on CT- respectively on 3 SENB-specimens. The mean values of a_{crit} calculated on the basis of mean $CTOD_{max}$-data are plotted. The test result number N and the standard deviation - SDEV - of a_{crit} is given in figure 8. The standard deviation of a_{crit} corresponds directly to the scatter in $CTOD_{max}$-data.

For every steel the lowest values of maximum allowable crack lengths a_{crit} were obtained if the results of CT-specimens were used. The $CTOD_{max}$-data of 3 SENB-samples resulted in a_{crit}-values which were up to 100% higher. If the results of side grooved specimens were used the differences in calculated a_{crit}-values were reduced for Fe E 470 and Fe E 460 steel. That means that for these steels the $CTOD_{max}$-data of 3 SENB-specimens are influenced strongly by side grooving. Whereas CT-specimens, with side grooves and without resulted, in the same $CTOD_{max}$-values. $CTOD_i$-values determined at the beginning of stable crack growth resulted in much lower values of a_{crit}:

$a_{crit} \cong 20,8 - 30,9$ mm for Fe E 470
$a_{crit} \cong 26,3 - 29,3$ mm for Fe E 460
$a_{crit} \cong 17,6$ mm for 20 MnMoNi 5 5

a_{crit}-values calculated on the basis of $CTOD_i$-data have some advantages. They are not affected by specimen geometry or specimen type. Whereas the grade of conservatism changes if geometry depended $CTOD_{max}$-data are used.

Wide plates can be used to check failure assessment methods. Therefore centre-notched-tension-loaded (CNT) samples were tested at RT. The thickness of the specimens were B = 30 mm for 20 MnMoNi 5 5 steel and B = 35 mm for the Fe E 470 and Fe E 460 steels. All CNT-specimens had a through-thickness notch. Wide plates of 20 MnMoNi 5 5 steel with different crack lengths (2a = 6,09 mm, 2a = 24,78 mm, 2a = 30,31 mm) and a constant width of W = 450 mm were tested. The wide plate of Fe E 460 steel had a crack length of 2a = 20,12 mm, it was 2a = 19,10 mm in the case of Fe E 470 steel and the width was W = 350 mm. All wide plates failed in a ductile manner and showed only stable growth on the fracture surfaces.

The failure loads of the CNT-samples were predicted by the "Engineering Approach" (13) using the assumption of plane stress behaviour. Four different calculations were performed for every steel based on the different J_R-curves shown in figures 4 to 6. Dahl et al. showed that the failure prediction based on the estimation scheme given by Kumar et al. (13) depends on the choice of parameters α and N of the Ramberg-Osgood law (15). Therefore an approximation was chosen of the true stress strain curves which agreed best in the upper hardening part.

Figure 9 shows a comparison of predicted failure load F_R and experimental failure load F_f of tested CNT-samples. The different slopes of J_R-curves influence the calculated maximum loads of the wide plates. While the J_R-curves of plain sided 3 SENB-samples resulted in the highest calculated failure loads the J_R-curves of side grooved CT-specimens give the lowest ones. Even then only one specimen of 20 MnMoNi 5 5 steel was predicted with some conservatism.

CONCLUSIONS

It was shown by fracture mechanics tests performed on steels with different strength levels using CT- and 3 SENB-specimens that the J-integral and CTOD values are comparable in the linear elastic regime of material behaviour up to the temperature T_i which describes the beginning of stable crack growth. The temperature T_i is not influenced by the specimen type. Fracture mechanics data J_i or δ_i determined at the beginning of stable crack growth by DC-potential technique are the same for CT- and 3 SENB-samples if

some scatter is taken into account. Within the temperature range where the specimens failed after some amount of stable crack growth, the 3 SENB-specimens resulted in higher J_{max} and $CTOD_{max}$-values.

Compared to plain sided CT-specimens all the 3 SENB-specimens resulted in J_R-curves with higher J-integral values and a steeper slope. The J_R-curves obtained from side grooved 3 SENB-samples showed only a small difference to those of CT-samples. While side grooving influenced the results of the 3 SENB-specimens dramatically the CT-specimens are affected only to a small amount.

It was shown that the maximum allowable crack length a_{crit} calculated by the CTOD-Design-Concept depends strongly on the specimen type. If specimen type affected CTOD values were used the grade of conservatism of the design concept changes. Therefore it seems to be better to use δ_i-data which are not influenced by the specimen geometry.

A comparison of predictions using the Engineering Approach and real experimental failure loads of some wide plates showed the effect of specimen type dependend J_R-curves. It is important that there is only a maximum difference of 15% if the calculation is done on the basis of plain sided 3 SENB-specimens instead of side grooved CT-specimens.

The results presented show that fracture mechanics values used for a safety analyses of a construction can be specimen type affected. It is to suppose that this behaviour is due to a 3-dimensional effect along the crack tip. A verification would be possible on the basis of finite-element computations which take stable crack growth into account.

SYMBOLS USED

a	= crack length
B	= specimen thickness
E	= Young's modulus
F	= load
J	= J-integral
J_{Ic}	= J-integral for crack initiation according to ASTM E 813
N	= parameter of Ramberg-Osgood law
N	= number of tests
SDEV	= standard deviation
W	= specimen width

20% SG = 20% side grooved

α = parameter of Ramberg-Osgood law

δ = CTOD-value

σ_{ys} = yield strength

σ_{UTS} = ultimate tensile strength

Δa = stable crack growth

ε_f = strain at fracture

REFERENCES

(1) Gudas, J.P. and Davis, D.A., J. Testing a. Eval. Vol. 10, No. 6, 1982, pp. 252-262.

(2) Jones, R.L., Barnes, P.J. and Duggan, T.V., Observations on R-Curve Determination, In: Advances in Fracture Research, Proceedings of the 6th Internat. Conf. on Frac. (ICF 6), Vol. 5, New Dehli, Edited by Valluri, S.R. et al., pp. 3409-3418.

(3) Garwood, S.J., Frac. Mech. ASTM STP 667, 1979, pp. 511-532.

(4) de Lorenzi, H.G. and Shih, C.F., Int. J. of Frac., Vol. 21, 1983, pp. 195-220.

(5) Dawes, M.G., A Method of Measuring Displacements and Rotational Factors in SENB Specimens, The Welding Inst. Res. Rep., No. 6, 1976.

(6) Zeislmair, H.C. and Dahl, W., Experimentelle Methoden zur Bestimmung von COD, In: Fortschrittsberichte VDI-Z-18, No. 10, Edited by Schwalbe, K.H., Düsseldorf 1981.

(7) Heuser, A. and Dahl, W., Materialprüfung, Vol. 26, No. 11, 1984, pp. 389-393.

(8) Heuser, A., Dormagen, D. and Dahl, W., Zur Problematik der Anwendung geometrieabhängiger COD-Werte für die Sicherheitsanalyse von Bauteilen mit dem Burdekin-Dawes Design Konzept, In: Proceedings Werkstoffprüfung 1984, DVM, 1985, Berlin, pp. 363-371.

(9) Sun, D.-Z., Dormagen, D. and Dahl, W., Steel Research, Vol. 56, 1985, No. 8, pp. 445-449.

(10) Shih, C.F., Andrews, W.R., de Lorenzi, H.G., German, M.D., von Stone, R.H. and Mowbray, D.F., Methodology for Plastic Fracture, Research Project 601-2/NP-1735, Final Rep. 1981, Electric Power Res. Inst., Palo Alto.

(11) Dahl, D., Dormagen, D., Ehrhardt, H., Hesse, W. and Twickler, R., Nucl. Eng. and Des., Vol. 87, 1985, pp. 83-88.

(12) Harrison, R.P., Loosemore, K. and Milne, I., Central Electricity Generating Board, Rep. No. R/H/R6, 1976.

(13) Kumar, V., German, M.D. and Shih, C.F., Fracture Handbook EPRI NP-1931, Res. Proj. 1237-1, General Electric Company, Schenectady, New York 1981.

(14) Guidance on some Methods for the Derivation of Acceptance Levels for Defects in Fusion Welded Joints, British Stand. PD 6493, 1980.

(15) Dahl, W., Hesse, W., Krabiell A. and Rosezin, H.J., Nucl. Eng. and Design, Vol. 76, 1983, pp. 309-318.

Steel	C	Si	Mn	P	S	Al	Cr	V	Mo	Zr
FeE 470	0,15	0,33	1,20	0,020	0,011	0,024	0,03	0,01	0,31	0,044
FeE 460	0,17	0,26	1,63	0,014	0,012	0,014	0,02	0,16	0,01	0,026
20MnMoNi 5 5	0,18	0,23	1,39	0,007	0,003	0,028	0,16	-	0,48	-
FeE 690	0,18	0,73	0,89	0,017	0,009	0,030	0,83	0,01	0,46	0,026

Steel	σ_{ys} [Nmm^{-2}]	σ_{UTS} [Nmm^{-2}]	ε_f [%]	RA [%]	CVN_{max} [J]
FeE 470	465	585	18,3	70	100
FeE 460	450	620	20,5	58,5	110
20MnMoNi 5 5	665	770	17,6	69,1	165
FeE 690	$\sigma_{0,2}$=740	840	17,0	65,0	85

Table 1 Chemical composition and mechanical properties of the steels investigated

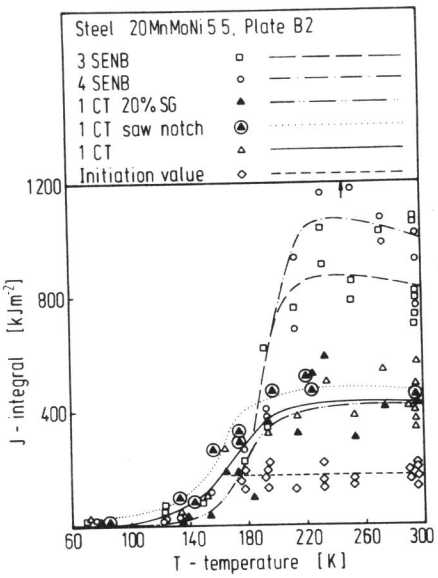

Figure 1 J-integral vs. temperature determinded on 20 MnMoNi 5 5

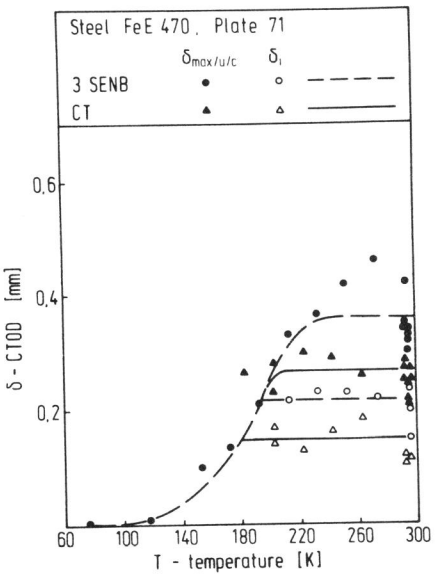

Figure 2 CTOD vs. temperature determined on Fe E 470

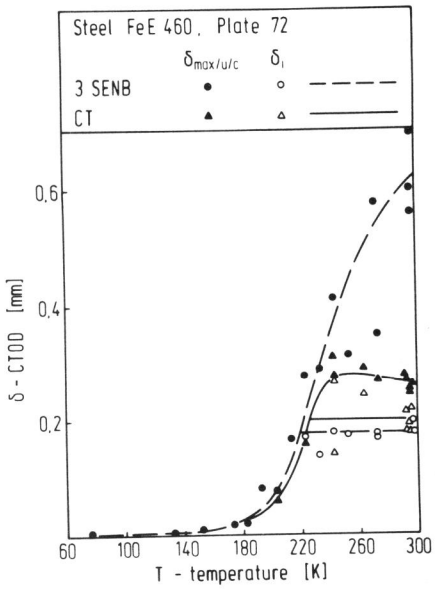

Figure 3 CTOD vs. temperature determined on Fe E 460

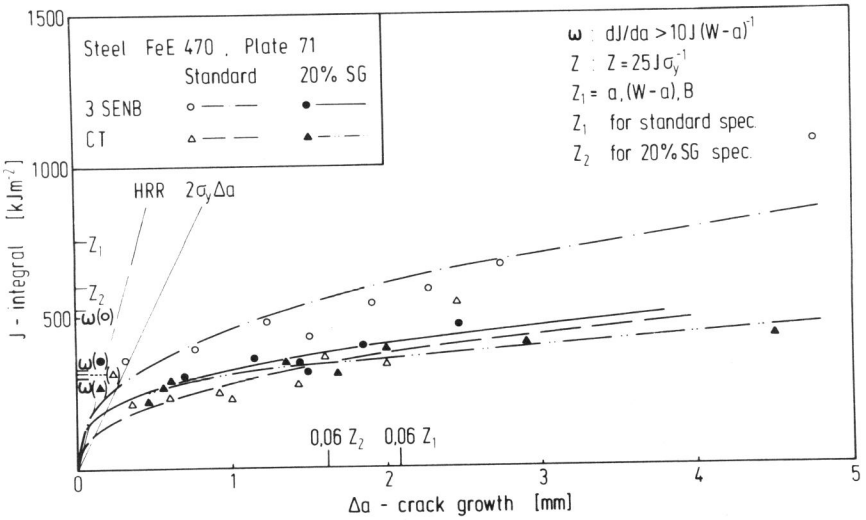

Figure 4 Comparison of J_R-curves determined on Fe E 470 by side grooved and plain sided 3 SENB- and CT-specimens

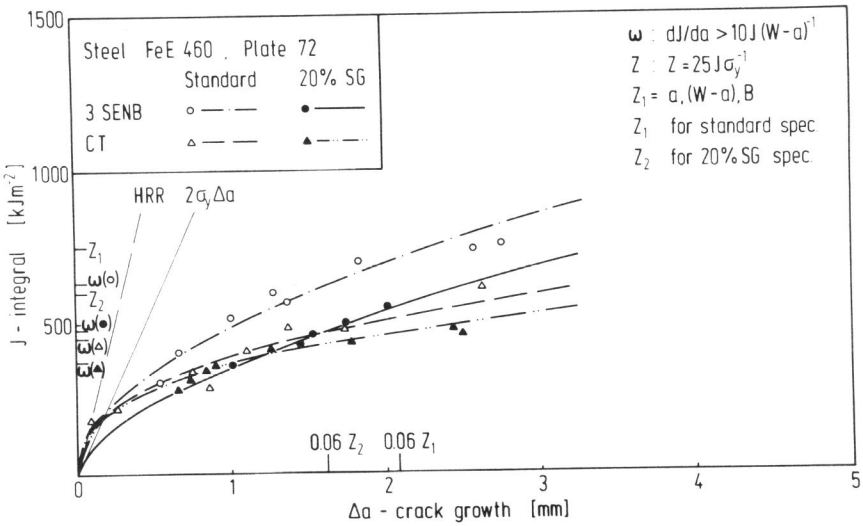

Figure 5 Comparison of J_R-curve determined on Fe E 460 by side grooved and plain sided 3 SENB- and CT-specimens

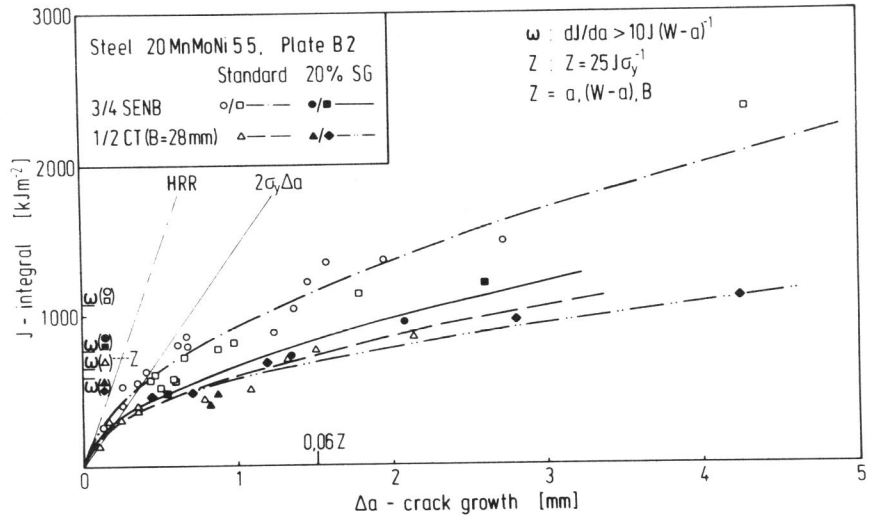

Figure 6 Comparison of J_R-curves determined on 20 MnMoNi 5 5 by side grooved and plain sided 3 SENB- and CT-specimens

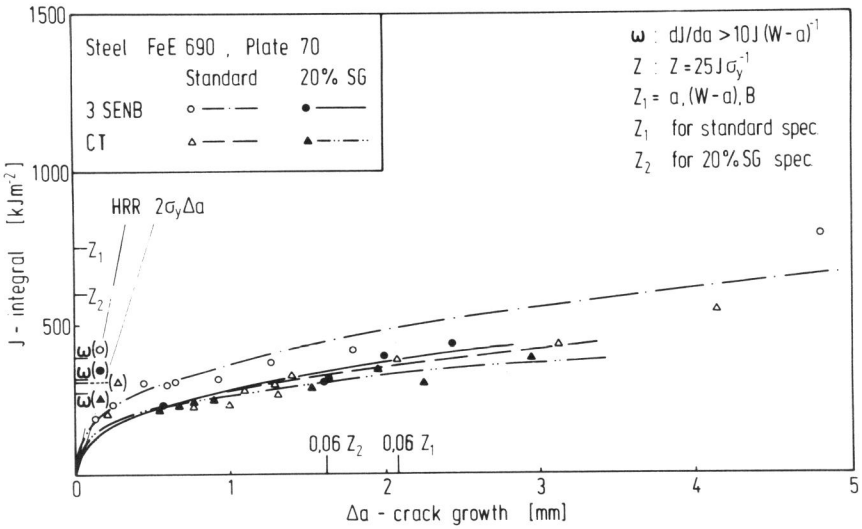

Figure 7 Comparison of J_R-curves determined on Fe E 690 by side grooved and plain sided 3 SENB- and CT-specimens

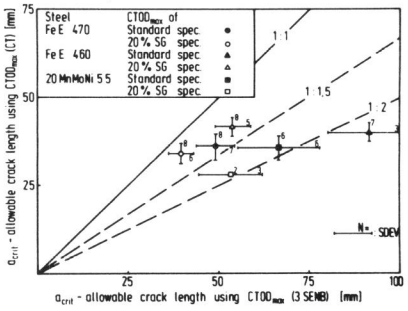

Figure 8 Comparison of a_{crit} according to (14)

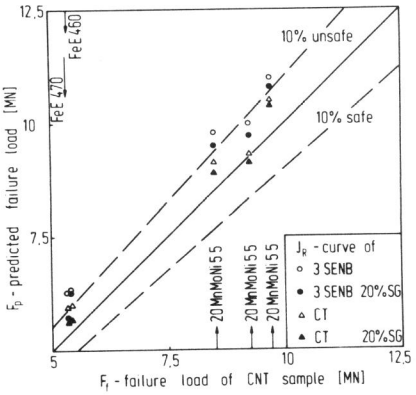

Figure 9 Comp. of pred. and test. failure load acc. to (13)